PB80-184245

A Mathematical Model for Calculating Electrical Conditions in Wire-Duct Electrostatic Precipitation Devices

Southern Research Inst.
Birmingham, AL

Prepared for

Industrial Environmental Research Lab.
Research Triangle Park, NC

15 Nov 76

U.S. Department of Commerce
National Technical Information Service
NTIS

TECHNICAL REPORT DATA
(Please read Instructions on the reverse before completing)

1. REPORT NO. EPA-600/J-77-172	2. JOURNAL ARTICLE
3.	PB80-184245
4. TITLE AND SUBTITLE: A Mathematical Model for Calculating Electrical Conditions in Wire-duct Electrostatic Precipitation Devices	5. REPORT DATE
	6. PERFORMING ORGANIZATION CODE
7. AUTHOR(S): J.R. McDonald, W.B. Smith, and H.W. Spencer III (SoRI); and L.E. Sparks (IERL-RTP)	8. PERFORMING ORGANIZATION REPORT NO.
9. PERFORMING ORGANIZATION NAME AND ADDRESS: Southern Research Institute, 2000 Ninth Avenue, South, Birmingham, Alabama 35205	10. PROGRAM ELEMENT NO. 1AB012
	11. CONTRACT/GRANT NO. 68-02-2114
12. SPONSORING AGENCY NAME AND ADDRESS: EPA, Office of Research and Development, Industrial Environmental Research Laboratory, Research Triangle Park, NC 27711	13. TYPE OF REPORT AND PERIOD COVERED: Journal article; 11/76
	14. SPONSORING AGENCY CODE: EPA/600/13

15. SUPPLEMENTARY NOTES: Published in Journal of Applied Physics, 48(6):2231-2243, June 1977. EPA/IERL-RTP author Sparks' mail drop is 61. His phone is 919/541-2925.

16. ABSTRACT

The article reports the devlopment of a new method of calculating electrical conditions in wire-duct electrostatic precipitation devices. The method, based on a numerical solution to the governing differential equations under a suitable choice of boundary conditions, accounts for the effect of space charge and is applicable over the entire range of current and voltage before sparkover. The procedure yields voltage-current characteristics and determines the electric potential and electric field strength as functions of position for each current and applied voltage. Predictions of the theory are compared with existing experimental data and the agreement is excellent.

17. KEY WORDS AND DOCUMENT ANALYSIS

a. DESCRIPTORS	b. IDENTIFIERS/OPEN ENDED TERMS	c. COSATI Field/Group
Pollution Measurement	Pollution Control	13B 14B
Electrostatic Precipitation	Stationary Sources	13H
Mathematical Models	Voltage-current Characteristics	12A
Electrical Properties		20C
Computation Charge Carriers		20L
Space Charge		

18. DISTRIBUTION STATEMENT: Release to Public	19. SECURITY CLASS *(This Report)*: Unclassified	21. NO. OF PAGES
	20. SECURITY CLASS *(This page)*: Unclassified	22. PRICE

EPA Form 2220-1 (9-73)

REPRODUCED BY NATIONAL TECHNICAL INFORMATION SERVICE U.S. DEPARTMENT OF COMMERCE SPRINGFIELD, VA 22161

EPA-600/J-77-172
JOURNAL ARTICLE

A mathematical model for calculating electrical conditions in wire-duct electrostatic precipitation devices

Jack R. McDonald, Wallace B. Smith, and Herbert W. Spencer III

Southern Research Institute, Birmingham, Alabama 35205

Leslie E. Sparks

Environmental Protection Agency, Research Triangle Park, North Carolina 27709
(Received 15 November 1976; accepted for publication 3 January 1977)

A new method is developed which can be used to calculate electrical conditions in wire-duct electrostatic precipitation devices. The method, based upon a numerical solution to the governing differential equations under a suitable choice of boundary conditions, accounts for the effect of space charge and is applicable over the entire range of current and voltage before sparkover. The procedure yields voltage-current characteristics and determines the electric potential and electric field strength as functions of position for each current and applied voltage. Predictions of the theory are compared with existing experimental data and the agreement is excellent.

PACS numbers: 85.50.−j, 41.10.Dq, 52.80.Hc

INTRODUCTION TO THE PROBLEM OF DETERMINING ELECTRICAL CONDITIONS

A theoretical calculation of current-voltage characteristics and the spatial dependence of the electric field in wire-duct electrostatic precipitation devices is important for the following reasons:

(a) It makes feasible a detailed analysis of current and voltage for various wire sizes, plate-to-plate spacings, and wire-to-wire spacings when the device is in the design stage.

(b) It can be incorporated into a computer model for electrostatic precipitation so that the effects of different operating conditions on performance can be analyzed before the device is constructed.

(c) It can be used to analyze electrical malfunctions in existing devices that are due to electrode misalignment.

Previous theoretical work found in the literature concerning wire-duct geometries has dealt mainly with determinations of the spatial dependence of the electric field. The solutions to the differential equations governing the electric field in wire-duct geometries are difficult to obtain because

(a) the differential equations do not lend themselves to simple analytical solutions as is the case with wire-pipe geometries,

(b) the differential equations are nonlinear,

(c) the electric field strength and space-charge density, due to free ions and charged particulate, are strongly related to one another and are both functions of position, and

(d) the free ions and charged particles have different mobilities which are functions of position.

Published solutions giving the spatial dependence of the electric field are based upon important approximations involving either the spatial dependence of the space-charge density or the mobilities of the charge carriers.

Experimental data on current-voltage characteristics are easily obtained and the literature abounds with such information for both clean-air and dirty-air situations. However, measurement of the electric field as a function of position is a difficult task and little information exists in the literature concerning this type of effort. Most methods employed in the past are not easily carried out experimentally and this leads to considerable uncertainty in the measured results. In addition, these methods have been applied mostly to clean-air cases where molecular ions are the only charge carriers.

Theoretical formulations by previous workers can be used to determine the electric field strength and space-charge density as functions of position, but no satisfactory technique has been suggested to accurately calculate the current-voltage characteristics. In this work a model and method are developed which can be used to calculate current-voltage characteristics in wire-duct geometries. The procedure, based upon the numerical technique suggested by Leutert and Böhlen,[1] accounts for the spatial effect of space charge and is applicable over the entire range of current and voltage where sparkover does not occur. In addition to the current-voltage characteristics, the method can be used to determine the electric potential and electric field strength as functions of position for each current and applied voltage. The predictions of the new formulation agree well with published experimental data.

Briefly, the technique consists of numerically solving Poisson's equation and the current continuity equation simultaneously and subject to the existing boundary conditions. Solutions are found for the electric potential and space-charge density. In an iteration procedure, the electric potential at the wire is adjusted until solutions are found that satisfy the boundary conditions. The space-charge density in the region of ionization near the discharge electrode is calculated and used as a boundary condition which is essential in the determination of current and voltage.

FORMULA SYMBOLS

V_0 applied voltage (V)

© 1977 American Institute of Physics

pgs. 2231-2243

S_x wire-to-plate spacing (m)

S_y one-half wire-to-wire spacing (m)

a radius of corona wire (m)

x coordinate position measured toward plate with the corona wire as origin (m)

y coordinate position measured parallel to plates with the corona wire as origin (m)

j_m measured average current density at the plate (A/m^2)

d a geometry factor which depends upon the ratio of S_x and S_y

b mobility of charge carriers ($m^2/V\,sec$)

i current per length of wire (A/cm)

D electric displacement ($A\,sec/m^2$)

ϵ_0 permittivity of air ($A\,sec/V\,m$)

$\mathbf{E}$ electric field strength (V/m)

V electric potential (V)

$\mathbf{j}$ current density (A/m^2)

ρ space-charge density ($Amp\,sec/m^3$)

j_i current density at the boundary of the ionized sheath (A/m^2)

I total current (A)

r_i radius of the ionized sheath (m)

l length of the corona wire (m)

ρ_i space-charge density at the boundary of the ionized sheath ($A\,sec/m^3$)

b_i effective charge carrier mobility at the boundary of the ionized sheath ($m^2/V\,sec$)

E_i electric field strength at the boundary of the ionized sheath (V/m)

A_{eff} effective plate area for each wire (m^2)

j_p average current denstiy at the plate (A/m^2)

$E'(r)$ static electric field strength in wire-cylinder geometry (kV/cm)

V_c corona starting voltage (kV)

r radial distance from the wire (cm)

r_c radius of the cylinder in wire-cylinder geometry (cm)

E_c electric field strength at the surface of the corona wire (kV/cm)

f roughness factor

δ relative density of air

T_0 absolute temperature of room air (°K)

T actual absolute temperature of air (°K)

P_0 normal atmospheric pressure (atm)

P actual atmospheric pressure (atm)

M ion amplification factor

ΔV_i potential across the ionizing sheath (V)

γ probability of avalanche electrons causing liberation of electrons from the passive electrode by ion impact and the photoelectric effect

α first Townsend coefficient (cm^{-1})

γ_p probability of avalanche electrons causing liberation of electrons from the passive electrode by the photoelectric effect.

PREVIOUS DETERMINATIONS OF ELECTRICAL CONDITIONS

Experimental measurements

Cooperman[2] used a dynamic-probe method in which precision ball bearing $\frac{1}{8}$ in. (3.18 mm) in diameter were shot at high velocities through the corona field parallel to the discharge wires. High velocities were necessary in order to avoid appreciable deflection of the balls in the corona field and to permit simultaneous determination of electric field strength and current density. The quantities measured were the charge acquired by the ball bearing and the time spent by the ball bearing in the field. From the measured quantities and the existing laws for particle charging, the values of electric field strength and current density could be deduced. The technique was checked quantitatively by a series of experiments in a coaxial cylinder corona. Agreement between theoretical curves and the experimental points was within 30% for all the tests conducted. In general, the agreement improved as the current density was increased.

Another series of measurements was made on the corona field in a wire-duct geometry. These experiments indicated that (1) the electric field strength reaches a minimum in the space between the discharge and passive electrodes, (2) the current density along the plate goes from a maximum value opposite a discharge wire to a minimum at a point midway between wires, and (3) the electric field strength at the plate is maximum between the wires. Indication (3) was later refuted by other investigators.[3–5]

Lagarias[6] conducted experimental studies using the dropping ball technique[6,7] in wire and plate precipitator assemblies in order to determine the electric-field-strength distributions. The effects of dust loading and variations in the wire-to-wire spacing were investigated. Steel spheres were allowed to fall by gravity through the corona field and the charge acquired by the spheres was measured. The electric field strength was calculated from the field charging equation where it was assumed that the spheres were fully charged. Experiments were also made in cylindrical geometry to check the reliability of the technique.

Measurements were made in wire-duct geometry under various conditions and the electric fields were mapped. Field-strength patterns indicated that increasing the discharge current increases the field strength between discharge electrodes whereas the field directly between the wire and the plates is substantially un-

changed. An unusually high-field-strength region was found to exist in the region between discharge electrodes and was attributed to space-charge effects. Changes in wire-to-wire spacing had little effect on the current per unit plate area but the current at any given voltage was greater for smaller wire-to-wire spacings. The primary effect of dust loadings was to increase the field strength because of the space charge generated by the slow-moving charged particles.

Penney and Matick[3] used a stationary-probe method to measure the potential distribution in dc corona fields. The probe consisted of a partially shielded fine wire with means for applying a countervoltage to the shield to overcome the effect of excess potential of the wire probe caused by the transfer of charge from corona ions. With this method, potentials could be measured accurately. Potential distributions measured in wire-cylinder geometries were in very good agreement with those calculated from theory.

The measurements were made in a wire-duct geometry consisting of wires spaced 6 in. (15.24 cm) from center to center midway between parallel grounded plates spaced 9 in. (22.86 cm) apart. Potential distributions were determined for various corona currents by changing applied voltages and wire sizes while keeping the electrode spacings constant. The results showed the influence of the corona current in increasing the electric field intensity near the passive electrode above the values which would occur for the electrostatic field. The curves of potential versus position measured with corona current had inflection points which indicate minimum values of the electric field intensity in the interelectrode space. Equipotential lines showed the potential distribution and electric field strength to be nearly uniform near the passive electrode with the uniformity being undisturbed by the effect of corona current.

Tassicker[5] used a "micro area boundary electrode" probe to measure the electric field strength and current density as functions of position at the collecting plate. The probe consisted of a small insulated circular electrode inserted into a large plane electrode which was grounded. The probe was connected in series with a current-measuring device and a variable voltage bias source. The current could be obtained directly and the electric field could be determined by varying the amplitude of the bias potential. In addition, the high-tension electrode system could be moved, while energized, relative to the grounded system in the x, y, and z directions. Thus, the current density and electric field could be measured at any position on the surface of the collecting plate.

Measurements were made with the probe on several different geometries, including wire duct. For wire-duct geometry, both the current density and electric field at the plate were found to be maximum opposite the discharge electrode. The measurements showed that the corona current caused a large increase in the electric field at the plate due to space-charge effects. Tests with positive and negative corona indicated only slight differences in the current-density and electric field patterns. These differences could be attributed to differing values of ion mobility.

Theoretical calculations

Even in the simplest case, that of zero space charge, calculation of the spatial dependence of the electric field is difficult for wire-duct geometries. By using a conformal mapping technique Cooperman[6] was able to transform the electric potential problem for the common geometry consisting of a wire positioned midway between parallel plates into that of a wire parallel to a single plate. The latter problem is easily solved by the method of images. The result, after superposition of potentials due to all the corona wires, is a series solution containing as many terms as there are corona wires in the precipitator. This solution is given by

$$V_s(x,y) = V_c\left[\sum_{m=-\infty}^{\infty} \ln\left(\frac{\cosh\pi(y-2mS_y)/2S_x - \cos(\pi x/2S_x)}{\cosh\pi(y-2mS_y)/2S_x + \cos(\pi x/2S_x)}\right)\right] \times\left[\sum_{m=-\infty}^{\infty} \ln\left(\frac{\cosh(\pi mS_y/S_x) - \cos(\pi a/2S_x)}{\cosh(\pi mS_y/S_x) + \cos(\pi a/2S_x)}\right)\right]^{-1}. \quad (1)$$

In practice the series converges rapidly and only a few terms need be evaluated. Since it completely ignores the space charge due to ions and charged particulate, this series is a purely electrostatic solution but gives an accurate representation of the electric field at voltages less than the critical voltage for the initiation of corona discharge.

In an effort to evolve a more general expression for the electric field, Cooperman[6] assumed that the space charge, consisting of free ions and charged particulate, is evenly distributed throughout any given transverse cross section within the precipitator. Separate solutions are found for the potential due to the corona wires in the absence of space charge and for the potential due to the space charge alone. Superposition of these solutions leads to the prediction of an electric field value near the plate about twice as great as the purely electrostatic solution. The complete expression for the potential is

$$V(x,y) = V_s(x,y) + \frac{j_m S_y \ln(d/a)}{\pi\epsilon_0 b V_0}(S_x^2 - x^2). \quad (2)$$

In an effort to avoid the shortcomings and difficulties inherent in seeking an analytical solution as was done by Cooperman, Leutert and Böhlen[1] used a relaxation technique[10-13] to numerically solve the governing differential equations. Poisson's equation and the current continuity equations were solved simultaneously and subject to the existing boundary conditions. In an iteration procedure, the space-charge density at the wire was adjusted until solutions were found that satisfied the boundary conditions of applied voltage and current density at the plate. Both the electric field strength and the space-charge density were found as functions of position. The major approximation, and one that may be unavoidable in practice, was the assumption that the motion of all the charge carriers can, on the average, be described by a single "effective mobility". The theoretical spatial dependence of the electric field was determined for a typical wire-duct geometry found in precipitators but no comparisons with experimental data were made.

Cooperman[6] has derived an approximate expression

relating current and voltage in wire-duct geometry which is valid for low current densities and applied voltages not too greater than the starting voltage. Starting with the equations for electrostatic field and using a perturbation method to account for the distortion of the electric field due to the presence of space charge, it was shown that, within the approximations, the current per centimeter of wire i is given by

$$i = \frac{b}{S_x^2 \log(d/a)} V(V - V_0). \tag{3}$$

Although this expression is useful for some applications, it cannot be used in general.

DEVELOPMENT OF THE DESCRIPTIVE EQUATIONS

For steady-state conditions and in the absence of magnetic effects, the equations defining the electric field in general are

$$\nabla \cdot \mathbf{D} = \rho \tag{4}$$

and

$$\nabla \cdot \mathbf{j} = 0, \tag{5}$$

where

$$\mathbf{D} = \epsilon_0 \mathbf{E}; \tag{6}$$

$$\mathbf{E} = -\nabla V, \tag{7}$$

and

$$\mathbf{j} = \rho b \mathbf{E}. \tag{8}$$

Equations (6) and (7) can be used with Eq. (4) to obtain an equivalent form,

$$\nabla^2 V = -\rho/\epsilon_0, \tag{9}$$

which is Poisson's equation. The problem is considered to be two-dimensional where edge effects and variations in V, E, and ρ parallel to the wires are neglected. Equation (9) can be written in discrete form in two-dimensional rectangular coordinates as

$$\frac{\Delta^2 V}{\Delta x^2} + \frac{\Delta^2 V}{\Delta y^2} = -\frac{\rho}{\epsilon_0}. \tag{10}$$

The continuity equation (5) can be transformed into an equation involving V and ρ by using Eqs. (4) and (6)–(8). Upon making the appropriate substitutions and using vector algebra one finds

$$\begin{aligned} \nabla \cdot \mathbf{j} &= \nabla \cdot (\rho b \mathbf{E}) = \rho b \nabla \cdot \mathbf{E} + b\mathbf{E} \cdot \nabla \rho + \rho \mathbf{E} \cdot \nabla b \\ &= \rho b(\rho/\epsilon_0) + b(-\nabla V) \cdot (\nabla \rho) + \rho(-\nabla V) \cdot (\nabla b) \\ &= 0 \end{aligned} \tag{11}$$

or

$$\rho^2 = \epsilon_0 (\nabla V) \cdot (\nabla \rho) + (\epsilon_0 \rho / b)(\nabla V) \cdot (\nabla b), \tag{12}$$

where both ρ and b depend upon position. Equation (12) can be written in a more convenient form as

$$\left(\frac{b}{\epsilon_0}\right)\rho^2 + \left(\frac{\partial b}{\partial x} E_x + \frac{\partial b}{\partial y} E_y\right)\rho + \left(\frac{\partial \rho}{\partial x} E_x + \frac{\partial \rho}{\partial y} E_y\right) b = 0, \tag{13}$$

which is a quadratic equation in ρ. Equation (13) can be written in discrete form in two-dimensional rectangular coordinates as

$$\left(\frac{b}{\epsilon_0}\right)\rho^2 + \left(\frac{\Delta b}{\Delta x} E_x + \frac{\Delta b}{\Delta y} E_y\right)\rho + \left(\frac{\Delta \rho}{\Delta x} E_x + \frac{\Delta \rho}{\Delta y} E_y\right) b = 0. \tag{14}$$

The solution of Eq. (14) for ρ is

$$\rho = \frac{\epsilon_0}{2b}\left\{-\left(\frac{\Delta b}{\Delta x} E_x + \frac{\Delta b}{\Delta y} E_y\right) \pm \left[\left(\frac{\Delta b}{\Delta x} E_x + \frac{\Delta b}{\Delta y} E_y\right)^2 - \frac{4b^2}{\epsilon_0}\left(\frac{\Delta \rho}{\Delta x} E_x + \frac{\Delta \rho}{\Delta y} E_y\right)\right]^{1/2}\right\}. \tag{15}$$

In order to determine the electrical characteristics of a wire-duct precipitator it is necessary to solve Eqs. (9) and (12), or Eqs. (10) and (15), simultaneously and subject to the existing boundary conditions. In solving the equations, the corona zone surrounding the discharge wire is considered only as a source of ions and high electric fields existing in this region are not treated in the calculation. The region outside the corona zone, where the electric field strengths are relatively low, is referred to as the space-charge zone and is assumed to contain unipolar ions.

NUMERICAL SOLUTIONS OF THE DESCRIPTIVE EQUATIONS

Formulation of the numerical solution

Figure 1 shows the basic area of interest in the precipitator for which Eqs. (10) and (15) are to be solved. Figure 2 also includes the geometry and nomenclature used in the numerical analysis. Due to the symmetry of the problem it is necessary to integrate only over the rectangle shown in Fig. 1 and then assert that the solu-

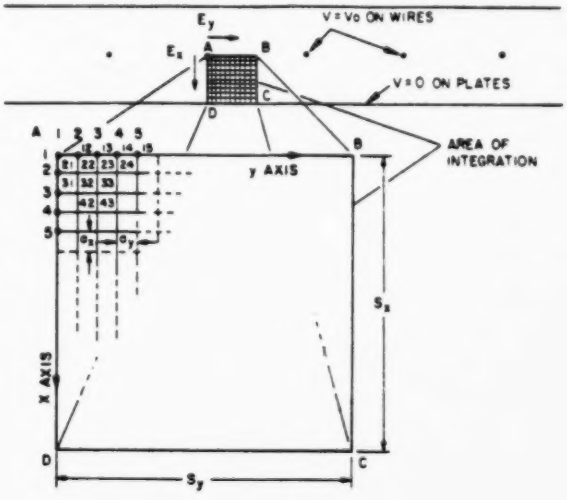

FIG. 1. Nomenclature used in the numerical analysis of the electrical conditions in wire-duct precipitators.

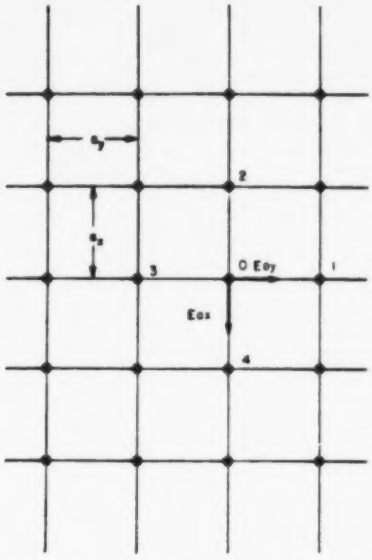

FIG. 2. Partial grid showing nomenclature used in the numerical analysis of the electrical conditions.

tions hold for all similar rectangles within the duct. In this manner the entire two-dimensional area can be taken into account. In the actual numerical procedure, occasions occur when values of V, E, and ρ from positions outside the rectangle are used. In this case it is justified to assign to the functions V, E, and ρ the same values they had at symmetrically located points within the area of the rectangle. This is necessary in order for the integration to include values of V and ρ which exist on the boundaries in such a way that they converge toward an exact solution along with the interior points.

In order to employ the method suggested by Leutert and Böhlen, the area of interest is divided into a fine rectangular grid as shown in Fig. 2. Point 0 is the point of interest for the following discussion. However, once V_0, E_0, and ρ_0 are calculated here, the label 0 is moved to a neighboring point and the calculation repeated. Each point in the grid would eventually become point 0.

From Fig. 2,

$$\frac{\Delta V_0}{\Delta x}=\frac{1}{2a_x}(V_4-V_2),$$

$$\frac{\Delta V_0}{\Delta y}=\frac{1}{2a_y}(V_1-V_3),$$

$$\frac{\Delta^2 V_0}{\Delta x^2}=\frac{V_4+V_2-2V_0}{a_x^2}, \tag{16}$$

and

$$\frac{\Delta^2 V_0}{\Delta y^2}=\frac{V_3+V_1-2V_0}{a_y^2}. \tag{17}$$

Equations (16) and (17) can be used in Eq. (10) and the resulting equation can be solved for V_0 to give

$$V_0=\frac{1}{2(a_x^2+a_y^2)}\left(a_y^2(V_2+V_4)+a_x^2(V_1+V_3)+\frac{a_x^2a_y^2\rho_0}{\epsilon_0}\right). \tag{18}$$

Again, from Fig. 2,

$$\frac{\Delta\rho_0}{\Delta x}=\frac{\rho_0-\rho_2}{a_x}, \tag{19}$$

$$\frac{\Delta\rho_0}{\Delta y}=\frac{\rho_0-\rho_3}{a_y}, \tag{20}$$

$$\frac{\Delta b_0}{\Delta x}=\frac{b_0-b_2}{a_x}, \tag{21}$$

and

$$\frac{\Delta b_0}{\Delta y}=\frac{b_0-b_3}{a_y}. \tag{22}$$

Equations (19)–(22) are based on difference intervals of $\Delta x=a_x$ and $\Delta y=a_y$, whereas Eqs. (16) and (17) are based on $\Delta x=2a_x$ and $\Delta y=2a_y$. Equations (19)–(22) are formulated in this manner because in the calculation of the initial space-charge-density grid the values at points 1 and 4 are unknown. Accurate derivatives will be obtained from Eqs. (19)–(22), provided the grid mesh is sufficiently small. An alternate approach is to use Eqs. (19)–(22) to establish the initial space-charge-density and mobility grids and then use equations based on $\Delta x=2a_x$ and $\Delta y=2a_y$ in subsequent calculations.

Finally, Eqs. (19)–(22) and Eq. (15) give

$$\rho_0=-\alpha\pm(\alpha^2+\beta)^{1/2}, \tag{23}$$

where

$$\alpha=\frac{\epsilon_0(2a_yb_0E_{0x}+2a_xb_0E_{0y}-a_yb_2E_{0x}-a_xb_3E_{0y})}{2a_xa_yb_0}$$

and

$$\beta=\frac{\epsilon_0(a_yE_{0x}\rho_2+a_xE_{0y}\rho_3)}{a_xa_y}.$$

Boundary conditions

The solutions to Eqs. (18) and (23) must be obtained subject to the existing boundary conditions. One set of boundary conditions for the area of interest in Fig. 1 is

(a) $\rho=\rho_0$ is the space-charge density near the wire, and hence $\rho=\rho_0$ at point A;

(b) $E_x=-(\Delta V/\Delta x)=0$ and $E_y=-(\Delta V/\Delta y)=0$ at points A and B;

(c) $V=0$ on the plate or along line CD;

(d) $E_x=-(\Delta V/\Delta x)=0$ along line AB;

(e) $E_y=-(\Delta V/\Delta y)=0$ along lines BC, CD, and AD;

(f) $\rho=j[-(\Delta V/\Delta x)b]^{-1}$ near the plate.

This particular set of boundary conditions is especially suited for determining a potential at the corona wire that would yield a given current density at the plate. The boundary conditions greatly simplify Eq. (23) along the lines AB, BC, AD, and CD and, in fact, make the calculation of the solutions to Eqs. (18) and (23) possible.

Determination of the space-charge density near the wire

Given an initial estimate of the potential grid, a space-charge-density grid can be generated from Eq. (23) provided the space-charge density near the wire is

known. An accurate estimate of the space-charge density near the wire must be made since this quantity is used as one of the boundary conditions that solutions to Eqs. (18) and (23) must satisfy.

If one assumes that the ionized sheath surrounding the wire can be approximated as cylindrical, the current density j_i at the boundary of the ionized sheath is given by

$$j_i = I/2\pi r_i l. \tag{24}$$

The quantity j_i can also be expressed in the form

$$j_i = \rho_i b_i E_i. \tag{25}$$

From Eqs. (24) and (25),

$$\rho_i = \frac{I/l}{2\pi b_i r_i E_i}. \tag{26}$$

Assuming continuity of current from the wire to the plate, we can write ρ_i in terms of the average current density j_p at the plates. The effective plate area A_{eff} for each wire can be given as

$$A_{eff} = 2(2S_y)l, \tag{27}$$

where $2S_y$ is the wire-to-wire spacing and the first factor of 2 enters the equation since there are two plates. Thus, j_p can be given by

$$j_p = I/A_{eff} = I/4S_y l. \tag{28}$$

From Eqs. (26) and (28) it can be shown that

$$\rho_i = \frac{2S_y j_p}{\pi b_i E_i r_i}. \tag{29}$$

The product $E_i r_i$ in Eq. (29) can be determined if some simplifying assumptions are made. It will be assumed that the radius of the region immedately near the wire where ionization occurs is approximately the same for both wire-duct and wire-cylinder geometries of comparable dimensions. This is reasonable since the characteristics of the region of ionization will depend primarily on the electric field near the wire, the gas composition, and the properties of the wire. Evidence in support of this assumption can be found in the fact that the corona starting voltage for a 20.32-cm wire and plate geometry in air with 0.277-cm-diam corona wires is only about 6% higher than for the corresponding wire-cylinder geometry.[14]

At corona onset, the current can be taken as zero and the electric field can be determined for a wire-cylinder geometry from the methods of electrostatics[15] as

$$E'(r) = \frac{V_c}{r \ln(r_c/a)}. \tag{30}$$

The electric field E_c at the surface of the wire at corona onset is

$$E_c = \frac{V_c}{a \ln(r_c/a)}. \tag{31}$$

Thus, the corona starting voltage can be expressed in the form

$$V_c = aE_c \ln(r_c/a). \tag{32}$$

The quantity E_c (kV/cm) has been determined semi-empirically by Peek[16] and is given by

$$E_c = f[30\delta + 9(\delta/a)^{1/2}], \tag{33}$$

where

$$\delta = \frac{T_0}{T}\frac{P}{P_0}. \tag{34}$$

For perfectly smooth clean wires, the roughness factor f is equal to unity. For corona wires in electrostatic precipitation practice, or for dirty scratched wires in the laboratory, f usually is between 0.5 and 0.7.[14]

If it is assumed that there is no space-charge distortion of the electric field within the ionized sheath, the electric field strength at the outer boundary of the sheath at corona onset is given by

$$E_i = \frac{V_c}{r_i \ln(r_c/a)}. \tag{35}$$

From Eqs. (32), (33), and (35),

$$E_i r_i = E_c a = af[30\delta + 9(\delta/a)^{1/2}]. \tag{36}$$

Equation (36) expresses the fact that, at corona onset where the space charge is negligible, the product $E'r$ is essentially constant. This is to be expected since the electrostatic field has a $1/r$ dependence and it is only slightly perturbed at corona onset.

Next, the effect on the product $E_i r_i$ resulting from applied voltages V_0 greater than V_c must be established. As is intuitively expected, increasing V_0 above V_c results in increased currents; however, the effects on space-charge density, radius of ionization, and electric field strength at the boundary of the ionized sheath are not so obvious.

It has long been known that, above the onset of steady positive corona in wire-cylinder geometry, Townsend's law[17] relating current i and overvoltage $V_0 - V_c$ of the form $V_0 - V_c \propto i/V_0$ applies over a considerable range. This relationship has been verified experimentally within fairly wide limits of potential variation irrespective of the gas composition or corona mechanism.[18–20] This law is deduced assuming a constant potential across a zone of limited constant ionizing radius.

Loeb[21] has shown that the assumptions upon which Townsend's law is derived imply two significant conclusions. First, the overvoltage $V_0 - V_c$ serves only to overcome and move the positive space charge and the corona operates at V_c. Second, the ion amplification factor M for ionization by electron impact must remain essentially constant. The constancy of the ion amplification factor has been experimentally established by Colli, Facchini, and Gatti.[22] This work showed that, over a voltage interval of about 1000 V, the ion amplification factor is practically independent of applied voltage and its value remains equal to the value at V_c.

Loeb[21,23] has developed a qualitative picture to explain how the current increases to give the increased space charge, while the potential across the ionizing sheath ΔV_i remains constant at a value established by V_c. Possible means of augmenting ion production are (a) increasing the ion amplification factor and/or γ, which increases the number of electrons generated at the cathode from ion impact and the photoelectric effect, as well as the time rate of successive events by increas-

ing ΔV_i, or (b) keeping the ion amplification factor, established at V_c, constant and merely increasing the number of multiplying sequences, corresponding to the threshold condition

$$\gamma M = \gamma \exp\left(\int_{r_i}^{s} \alpha \, dr\right) = 1, \tag{37}$$

per unit area of electrode surface. In Eq. (37), α is the first Townsend coefficient, which represents the number of new electrons created per centimeter path in the field direction in the avalanche process occurring in the ionized sheath. Changes by mechanism (a) would involve increasing the potential for active ionization above the value ΔV_i established at V_c and increasing r_i. If the increase were of any magnitude over an extended voltage regime, this would at once be detected through failure of Townsend's law and of measurements such as those of Colli, Facchini, and Gatti.

The qualitative description given by Loeb is based on mechanism (b). At a steady current, assume that the potential is raised by a very slight amount, ΔV_0. This at once increases the ion amplification factor for each electron avalanche. Thus, the number of photons creating the γ_p, or its equivalent, is at once increased. These lead to more and new electron avalanches, which originate from areas on the cathode that were not emitting avalanche successions before. Thus, new avalanches are launched and the surface density of ionizing avalanches increases. On arrival at the anode more positive ions are created. As these move out of the ionizing sheath, the space charge begins to increase near the temporarily extended r_i above that which existed before ΔV_0 was applied. By the time the ion increase reaches the cathode, the potential drop across the space charge has risen to $V_0 + \Delta V_0 - \Delta V_i$, restoring the potential across r_i to ΔV_i and placing the new potential increment across the space charge.

In Loeb's description, the space charge and current will increase with increasing values of V_0. However, ΔV_i and the ion amplification factor will in large measure be unchanged except for a small instantaneous fluctuation, lasting perhaps some 10 μsec. This description was developed mathmatically by Colli, Facchini, Gatti, and Persono[24] in a quantitative theory and proven to be correct. The theory predicted the regular instantaneous fluctuations which were seen experimentally and suggested by Loeb's qualitative analysis.

From the work of Loeb and of Colli, Facchini, Gatti, and Persono, it can be concluded that, once steady corona is initiated at V_c, the product $E_i r_i$ is established and remains essentially constant over a wide range of increased applied voltages and currents. Thus, from Eqs. (29) and (36), the space-charge density at the boundary of the ionized sheath is given for all currents by

$$\rho_i = \frac{2S_y j_p}{\pi b_i a f[30\delta + 9(\delta/a)^{1/2}]} \times 10^{-3}, \tag{38}$$

where all the quantities are measured in mks units except a, which is in cgs units. Also, since the calculation of electrical conditions in the present work is concerned only with the low-field regions outside the ionized sheath, ρ_i may be taken to be point-charge density located at the center of the corona wire.

Description of the numerical procedure

Equations (18) and (23) are used to generate potential and space-charge-density grids which are calculated alternately, one from the other, in an iterative scheme. The initial values that are used for the potential grid are obtained by estimating the applied voltage V_0 that would produce a given average current density j_p at the plate using Cooperman's electrostatic series equation. Once an initial estimate of the potential grid is established, the space-charge-density grid can be calculated using Eqs. (38) and (23). The values of the space-charge density at points along the lines AB and AD are calculated first, with the aid of the boundary conditions, and then the values for the interior points are obtained. After obtaining the initial potential and space-charge values, a new potential grid is calculated from the space-charge grid. Then, a new space-charge grid is calculated from the new potential grid. This scheme is continued until the potential grid converges. If the potential grid converges and the computed average current density at the plate equals the chosen boundary value, the simultaneous solution of Eqs. (10) and (15) has been found. If the boundary condition on the current density is not met, the potential at the wire is adjusted and the entire procedure is started again by generating a new space-charge-density grid.

In summary, the steps in the numerical procedure are outlined as follows.

(a) Estimate the potential at the wire and calculate V at every point in the grid using Eq. (1).

(b) Calculate ρ at every point in the grid using Eq. (23), where the space-charge density at the wire is given by Eq. (38).

(c) Recalculate V at every point in the grid using Eq. (18).

(d) Repeat steps (b) and (c) alternately until each value of V in the potential grid changes negligibly from its previous value.

(e) Check to see if the computed average current density at the plate equals the desired value. If they agree, then the solution has been obtained. If they do not agree, adjust the potential at the wire and start the calculation over at step (b) above.

A computer program has been written which determines the electrical conditions in wire-duct geometries by simultaneous solution of Eqs. (10) and (15) using the new method and the above procedure. The convergence criteria are that each value of potential in the grid be within 1 V of its previous value and that the current density be within 1% of the desired value.

RESULTS AND COMPARISON WITH EXPERIMENTAL DATA

Figures 3–10 show theoretical trends predicted by the new method. The figures indicate the effects on the electrical conditions caused by varying the geometrical factors. In all of these figures the values of δ and f are taken to be unity.

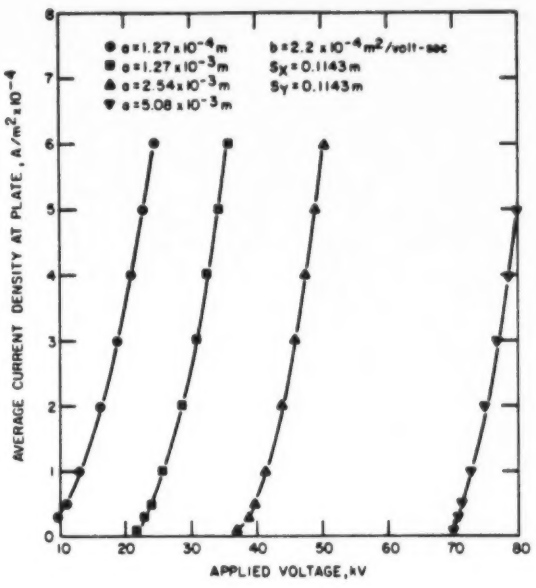

FIG. 3. Theoretical curves showing the effect of wire size on voltage-current characteristics.

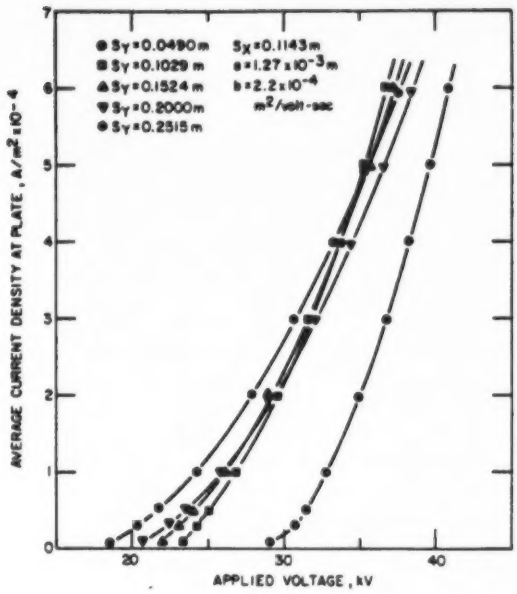

FIG. 5. Theoretical curves showing the effect of wire-to-wire spacing on voltage-current characteristics.

Figures 3–5 demonstrate the effects of wire size, plate-to-plate spacing, and wire-to-wire spacing on voltage-current characteristics. Figure 3 shows that an increase in wire size leads to a higher starting voltage and lower currents for the same applied voltages. Figure 4 demonstrates that increasing the plate-to-plate spacing has only a slight effect on raising the starting voltage but leads to a large drop in current for the same applied voltage. Figure 5 indicates that the wire-to-wire spacing has little effect on voltage-current characteristics over a wide range of values.

Figures 6–8 illustrate how the average electric field at the plate E_p and the average electric field between the electrodes E_a vary as a function of the average current density at the plate for different wire sizes, plate-to-

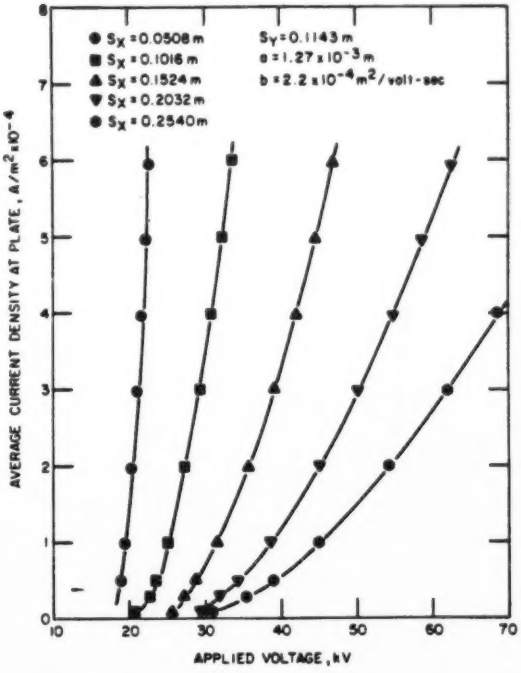

FIG. 4. Theoretical curves showing the effect of plate-to-plate spacing on voltage-current characteristics.

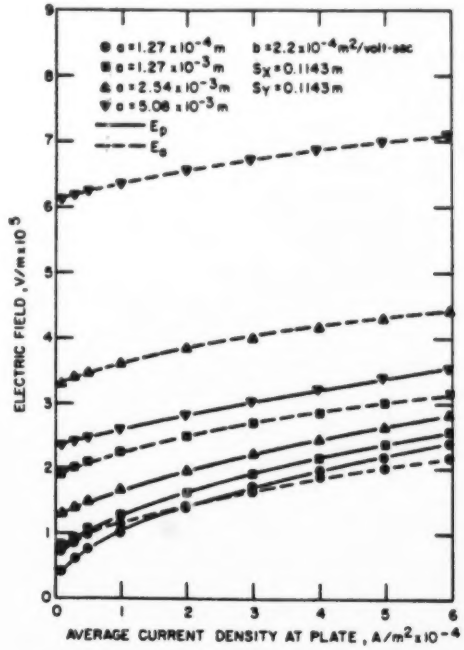

FIG. 6. Theoretical curves showing the effect of wire size on the electric field and current density.

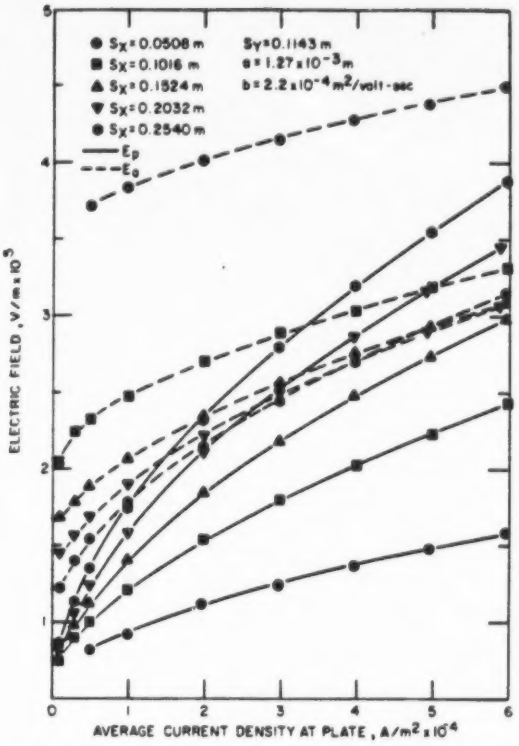
● S_X = 0.0508 m
■ S_X = 0.1016 m
▲ S_X = 0.1524 m
▼ S_X = 0.2032 m
● S_X = 0.2540 m
S_Y = 0.1143 m
a = 1.27 x 10⁻³ m
b = 2.2 x 10⁻⁴ m²/volt-sec
E_p
E_o
ELECTRIC FIELD, V/m x 10³
AVERAGE CURRENT DENSITY AT PLATE, A/m² x 10⁴

FIG. 7. Theoretical curves showing the effect of plate-to-plate spacing on the electric field and current density.

plate spacings, and wire-to-wire spacings. Figure 6 shows that for the same average current density at the plate the average electric field at the plate increases slowly with increasing wire size. Figure 7 demonstrates

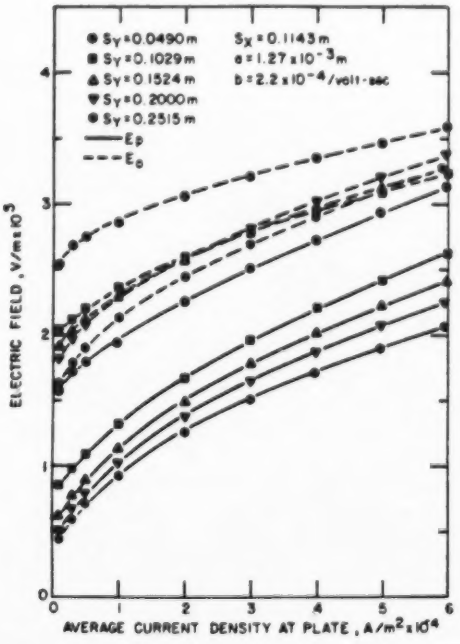
● S_Y = 0.0490 m
■ S_Y = 0.1029 m
▲ S_Y = 0.1524 m
▼ S_Y = 0.2000 m
● S_Y = 0.2515 m
S_X = 0.1143 m
a = 1.27 x 10⁻³ m
b = 2.2 x 10⁻⁴ m²/volt-sec
E_p
E_o
ELECTRIC FIELD, V/m x 10³
AVERAGE CURRENT DENSITY AT PLATE, A/m² x 10⁴

FIG. 8. Theoretical curves showing the effect of wire-to-wire spacing on the electric field and current density.

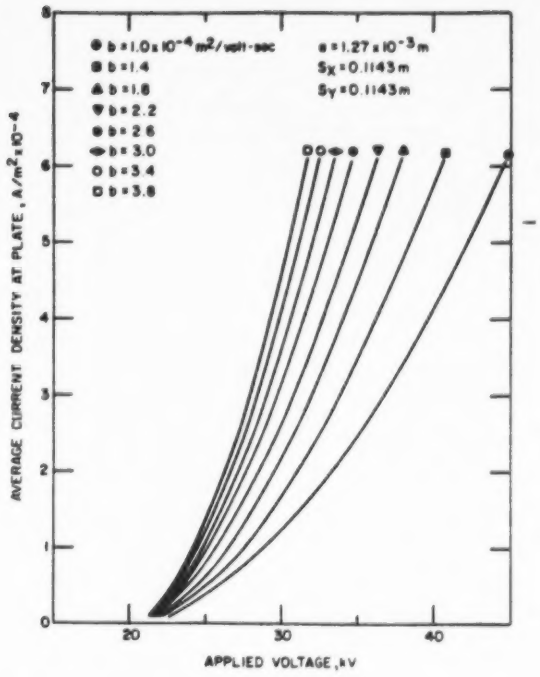
● b = 1.0 x 10⁻⁴ m²/volt-sec
■ b = 1.4
▲ b = 1.8
▼ b = 2.2
● b = 2.6
◆ b = 3.0
○ b = 3.4
□ b = 3.8
a = 1.27 x 10⁻³ m
S_X = 0.1143 m
S_Y = 0.1143 m
AVERAGE CURRENT DENSITY AT PLATE, A/m² x 10⁻⁴
APPLIED VOLTAGE, kV

FIG. 9. Theoretical curves showing the effect of effective mobility on voltage-current characteristics.

that for the same average current density at the plate the average electric field at the plate increases rapidly with increasing plate-to-plate spacing. Figure 8 indicates that the wire-to-wire spacing has only a small

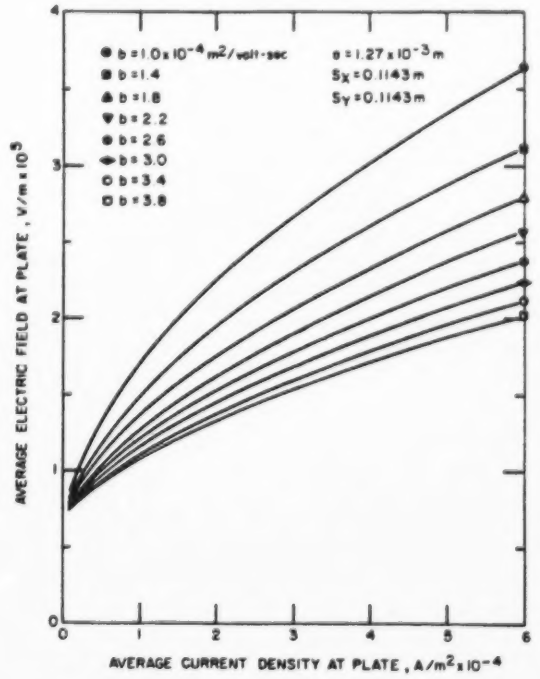
● b = 1.0 x 10⁻⁴ m²/volt-sec
■ b = 1.4
▲ b = 1.8
▼ b = 2.2
● b = 2.6
◆ b = 3.0
○ b = 3.4
□ b = 3.8
a = 1.27 x 10⁻³ m
S_X = 0.1143 m
S_Y = 0.1143 m
AVERAGE ELECTRIC FIELD AT PLATE, V/m x 10³
AVERAGE CURRENT DENSITY AT PLATE, A/m² x 10⁻⁴

FIG. 10. Theoretical curves showing the effect of effective mobility on the electric field and current density.

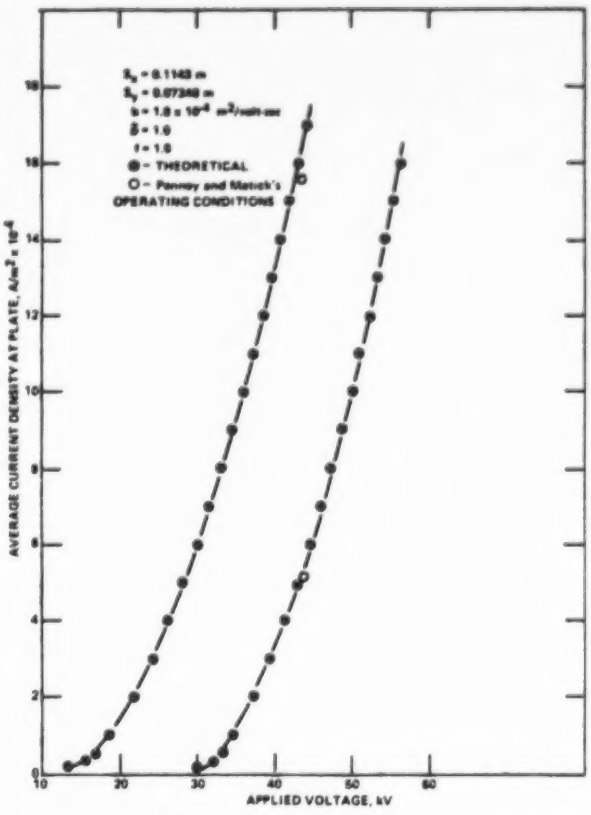

FIG. 11. Theoretical voltage-current characteristics for the geometries used by Penney and Matick (Ref. 3).

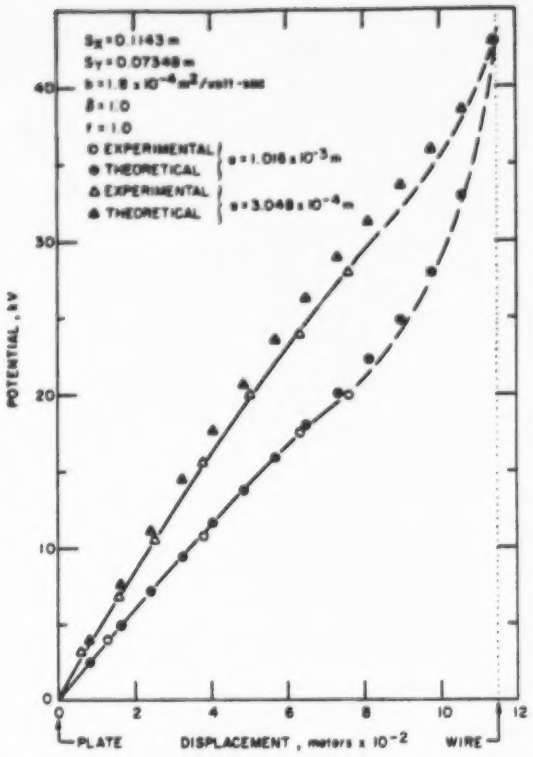

FIG. 12. Theoretical and experimental potential profiles along a line from the corona wire to the plate.

effect on the average electric field at the plate for any given average current density at the plate.

Figures 9 and 10 indicate the effect of different values of effective mobility on the voltage-current characteristics and the average electric field at the plate versus average current density at the plate. When particles are introduced into a precipitator, some of the molecular ions transfer their charge to particles and the total current and space charge are due to both ions and much less mobile particles. Normally the particles contribute very little to the total current due to their low mobilities but they can have an appreciable space-charge effect. It has been shown[25] that the effect due to particulate space charge can be associated with a lowering of the effective mobility that would exist if only molecular ions were present. Thus, the curves given in Figs. 9 and 10 can be used to analyze space-charge effects due to particles through the lowering of the effective mobility.

From Fig. 9, it can be seen that if the ion mobility for negative corona is 2.6×10^{-4} m²/V sec and the introduction of particles reduces the effective mobility to 1.4×10^{-4} m²/V sec, an increase of approximately 6 kV is required to produce a current density of 60 nA/cm². From Fig. 10, it can be seen that for the same current density the introduction of particles causes an increase in the electric field at the plate and this effect becomes more pronounced as the effective mobility is decreased. As of yet, no experimental or theoretical information exists on values of effective mobility as a function of particulate loading and particle size distribution. Thus, values of effective mobility corresponding to conditions encountered in practical situations are unknown.

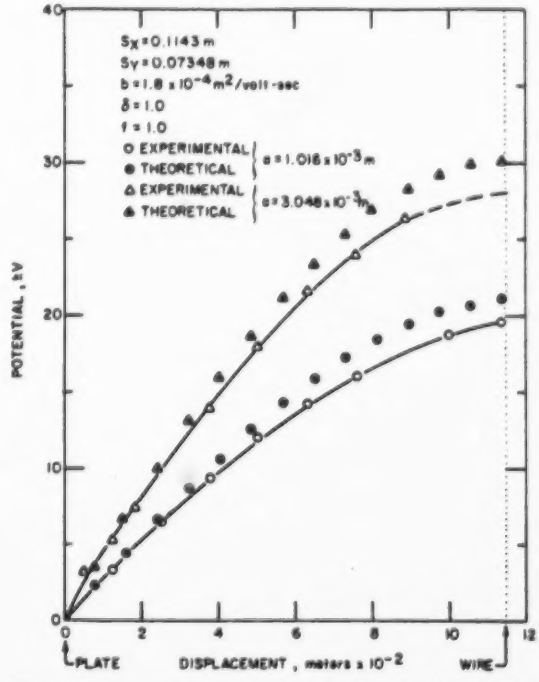

FIG. 13. Theoretical and experimental potential profiles along a line from a point midway between the wires to the plate.

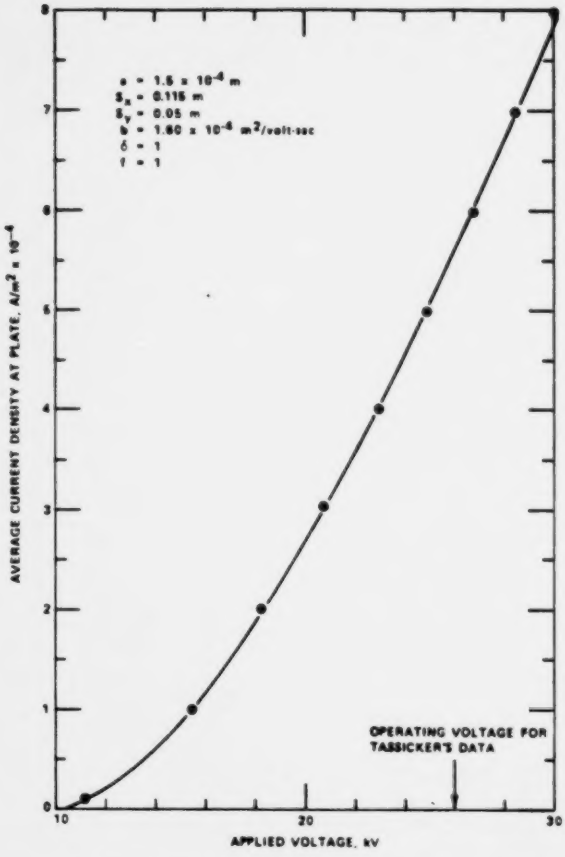
a = 1.5 x 10⁻⁴ m
S_x = 0.115 m
S_y = 0.05 m
b = 1.80 x 10⁻⁴ m²/volt-sec
δ = 1
f = 1
AVERAGE CURRENT DENSITY AT PLATE, A/m² x 10⁻⁴
APPLIED VOLTAGE, kV
OPERATING VOLTAGE FOR TASSICKER'S DATA

FIG. 14. Theoretical voltage-current characteristics for the geometry used by Tassicker (Ref. 5).

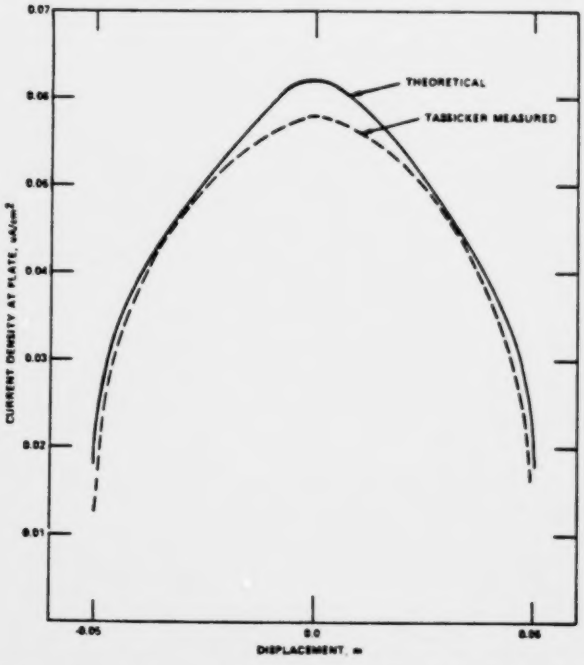

FIG. 15. Theoretical and experimental current density at the plate as a function of displacement.

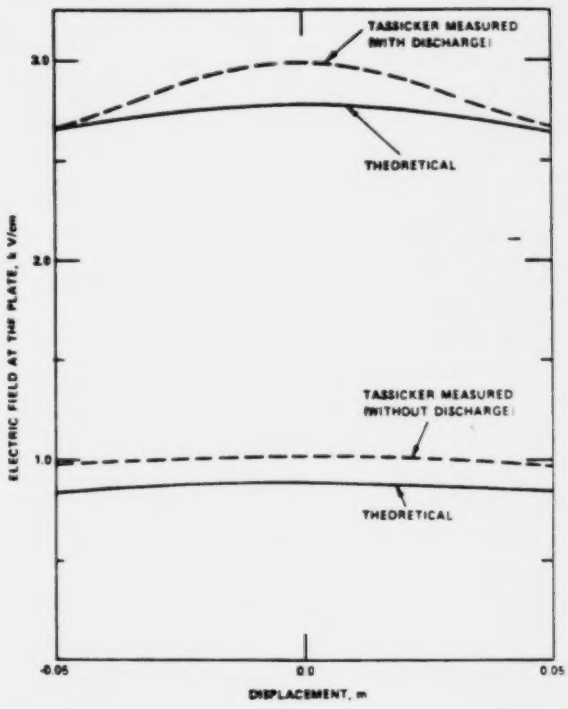

FIG. 16. Theoretical and experimental electric field at the plate as a function of displacement.

Figures 11–13 compare some experimental results reported by Penney and Matick[3] with those predicted by the new method. The theoretical results were obtained using a 15×10 grid in the numerical procedure. Figures 11 and 12 give theoretical voltage-current curves for two of the geometries used by Penney and Matick along with the experimental operating condition in each case. An effective mobility of 1.8×10^{-4} m²/V sec yields voltage-current curves which predict the experimental operating conditions within 2% and the corresponding potential profiles within 10% at all points. The value of 1.8×10^{-4} m²/V sec is consistent with published values of ion mobility characteristic of negative corona discharge in air. Figures 12 and 13 show that excellent argreement between the theory and experiment exists for the potential profiles from the wire to the plate and from a point midway between the wires to the plate.

Figures 14–16 compare some experimental data obtained by Tassicker[5] with those predicted by the new method. The experimental data are for positive corona with an applied voltage of 26 kV. The theoretical results were obtained using a 15×15 grid in the numerical procedure. Figure 14 is a theoretical voltage-current curve for the geometry used in the experiments. An effective mobility of 1.6×10^{-4} m²/V sec was used in determining the experimental values of electric field and this value was used in the theoretical calculations

In Figs. 15 and 16 corona wires are located directly across from the points $x=-0.1$, 0, and 0.1 m at the plate. Positions $x=-0.05$ and 0.05 correspond to positions at the plate, midway between corona wires. The current density and electric field are a maximum

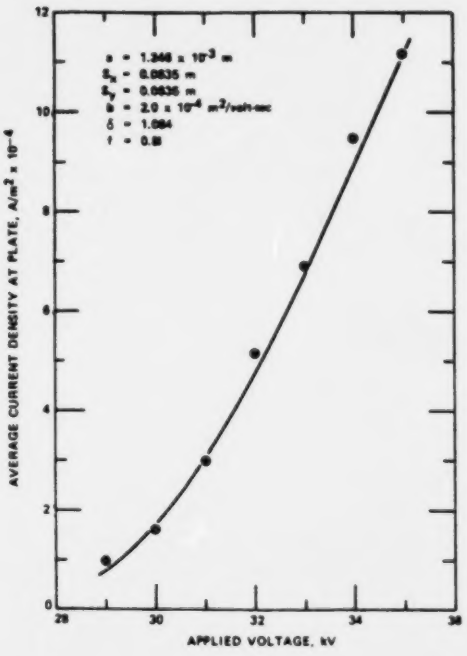

FIG. 17. Theoretical and experimental voltage-current characteristics for a laboratory scale precipitator.

directly across from a corona wire according to both the experimental data and the theory. The agreement between experiment and theory is within 8%.

Figure 17 shows experimental voltage-current data obtained during the present study from a laboratory precipitator using negative corona in laboratory air. The figure also shows the theoretical curve calculated using a 15×15 grid in the numerical procedure. The data were taken with dirty wires and this is reflected in the choice of $f=0.81$. An effective mobility of 2.0×10^{-4} m^2/V sec was used in the theory. The agreement between the experimental data and theory is quite good considering the size of the precipitator and the fact that some misalignment of electrodes existed.

In applying the theory, some uncertainty exists in the choice of values to use for the effective mobility and the roughness factor. There has been a wide range of experimental values [$(1.1-2.2)\times10^{-4}$ m^2/V sec] reported in the literature for the effective mobility of molecular ions created in a corona discharge in laboratory air.[36,37] Since the ionic species will differ for positive and negative corona discharge, different effective ion mobilities should be expected. In addition, small quantities of particulate matter and moisture in unfiltered laboratory air can cause a reduction in the effective mobility that would exist without their presence. Comparisons of theoretical and experimental results presented in this work indicate that values of effective mobility in the range $(1.6-2.0)\times10^{-4}$ m^2/V sec are suitable for theoretical studies of negative and positive corona discharge in laboratory air and that this range of values will not have too severe an effect on theoretical predictions. In industrial applications, flue gases will have various compositions that differ from laboratory air. Effective ion mobilities for flue gases must be obtained by synthesizing the gas composition in the laboratory or making an *in situ* determination in which particulate matter is filtered out of the gas. Use of the theory to accurately predict electrical conditions for corona discharge in a flue gas would depend on a reasonable knowledge of the effective ion mobility.

The value chosen for the roughness factor can have a significant effect on the predictions of the theory because it affects the starting voltage and the charge density. The roughness factor lies approximately in the range 0.5—1.0 and a 0.1 change in value will result in considerably different predictions by the theory. For clean unscratched wires that are used in laboratory air, the roughness factor can be taken as unity with good results. If the wires are dirty, scratched, or used in a dirty environment, the roughness factor will be less than unity and may be difficult to estimate correctly.

SUMMARY AND CONCLUSIONS

A new method has been presented which is capable of predicting the electrical conditions in electrostatic precipitation devices with wire-duct geometry. The method differs from previous work in that the voltage-current characteristics can be determined theoretically as well as the potential and electric fields. The method also has the capability of treating the effective mobility as a function of position should this information become available in the future.

Comparisons of the predictions of the theory with existing experimental data indicate that the theory can be used accurately in the design of electrostatic precipitation devices with wire-duct geometry. The theory can be used to analyze the effect of various geometrical configurations on the voltage-current characteristics and the electric field distributions. In this manner the average current density and average electric field near the plate can be optimized to yield the best collection by electrostatic precipitation. In addition, space-charge effects due to the introduction of particles can be estimated by an appropriate lowering of the effective mobility.

ACKNOWLEDGMENTS

The work described in this paper was supported by the Control Systems Laboratory, Environmental Protection Agency, Research Triangle Park, N.C., under Contract No. 68-02-2114, Dr. Leslie E. Sparks, Project Officer.

[1]G. Leutert and B. Böhlen, Staub 32 (No. 7), 27 (1972).
[2]P. Cooperman, Trans. Am. Inst. Electr. Eng. 1 75, 64 (1956).
[3]G.W. Penney and R.E. Matick, Trans. Am. Inst. Electr. Eng. 1 79, 91 (1960).
[4]J.S. Lagarias, Trans. Am. Inst. Electr. Eng. 78, 427 (1959).
[5]O.J. Tassicker, Ph.D. dissertation (Wallongong University College, University of South Wales, 1972), Chap. 6, p. 159 (unpublished).
[6]M. Pauthenier and M. Moreau-Hanot, J. Phys. Radium 6, 257 (1935).
[7]G.W. Penney and J.G. Hewitt, Trans. Am. Inst. Electr. Eng. 1 77, 319 (1958).

[8]P. Cooperman (unpublished).
[9]P. Cooperman, Trans. Am. Inst. Electr. Eng. 79, 47 (1960).
[10]S. Flügge, *Handbuch der Physik* (Springer-Verlag, Berlin, 1958), Vol. 16, p. 248.
[11]K.J. Burns and P.J. Lawrenson, *Analysis and Computation of Electrical and Magnetic Field Problems* (Pergamon, Oxford, 1963), p. 251.
[12]A. Ralston and H.S. Wilf, *Mathematical Methods for Digital Computers* (Wiley, New York, 1960), p. 144.
[13]D. Young, Trans. Am. Math. Soc. 76, 92 (1954).
[14]H.J. White, *Industrial Electrostatic Precipitation* (Addison-Wesley, Reading, Mass., 1963), p. 92.
[15]L.B. Loeb, *Fundamentals of Electricity and Magnetism* (Wiley, New York, 1947 (Dover, New York, 1961), p. 217.
[16]F.W. Peek, Jr., *Dielectric Phenomena in High Voltage Engineering*, 3rd ed. (McGraw-Hill, New York, 1929), p. 64.
[17]J.S. Townsend, Philos. Mag. 28, 83 (1914).
[18]S. Werner, Z. Phys. 90, 356 (1934).
[19]S. Werner, Z. Phys. 92, 705 (1934).
[20]C.G. Miller and L.B. Loeb, J. Appl. Phys. 22, 499 (1951).
[21]L.B. Loeb, Phys. Rev. 90, 144 (1953).
[22]L. Colli, U. Facchini, and E. Gatti, Rev. Sci. Instrum. 23, 621 (1952).
[23]L.B. Loeb, *Electrical Coronas* (University of California Press, Berkeley, 1965), p. 46.
[24]L. Colli, U. Facchini, E. Gatti, and A. Persano, J. Appl. Phys. 25, 429 (1954).
[25]S. Oglesby, Jr., and G.B. Nichols, *A Manual Electrostatic Precipitator Technology* (Southern Research Institute, Birmingham, Ala., 1970), Vol. 1, p. 58.
[26]B.Y.H. Liu, K.T. Whitby, and H.H.S. Yu, J. Appl. Phys. 38, 1592 (1967).
[27]J. Bricard, M. Cabane, G. Madelaine, and D. Vigla, *Aerosols and Atmospheric Chemistry*, edited by G.M. Hidy (Academic, New York, 1972), p. 27.